ACS APPLIED MATERIALS & INTERFACES

Research Article

Cite This: ACS Appl. Mater. Interfaces 2018, 10, 32313−32322

www.acsami.org

Ion Removal Performance, Structural/Compositional Dynamics, and Electrochemical Stability of Layered Manganese Oxide Electrodes in Hybrid Capacitive Deionization

Bryan W. Byles,[†] Brendan Hayes-Oberst,[†] and Ekaterina Pomerantseva*

Department of Materials Science and Engineering, Drexel University, Philadelphia, Pennsylvania 19104, United States

Supporting Information

ABSTRACT: Hybrid capacitive deionization (HCDI) is a derivative of capacitive deionization (CDI) method for water desalination, in which one carbon electrode is replaced with a redox-active intercalation electrode, resulting in substantial improvements in ion removal capacity over traditional CDI. The search for high-performing intercalation host compounds is ongoing. In this study, two-layered manganese oxides (LMOs), with sodium (Na-birnessite) and magnesium (Mg-buserite) ions stabilizing the interlayer region, were for the first time evaluated as HCDI electrodes for the removal of ions from NaCl and $MgCl_2$ solutions to understand structural/compositional dynamics and electrochemical stability of LMO electrodes over extended cycling. Both materials demonstrated excellent initial ion removal performance with the highest capacities of 37.2 mg g^{-1} (637 μmol g^{-1}) exhibited by Mg-buserite in NaCl solution and 50.2 mg g^{-1} (527 μmol g^{-1}) exhibited by Na-birnessite in $MgCl_2$ solution. The performance decay observed over the course of 200 ion adsorption/ion release cycles was attributed to two major phenomena: oxidation of carbon electrode and evolution of the structure/composition of LMO electrodes. The latter involves disorder in stacking of Mn−O layers and changes in the interlayer spacing/interlayer ions reflecting the composition of the solution being desalinated. This work highlights the importance of understanding the interactions between the HCDI electrodes and solutions containing different ions and the structural analysis of redox-active material in intercalation electrodes over the course of operation for gaining insight into the fundamental processes governing desalination performance and developing next-generation HCDI systems with long-term electrochemical stability.

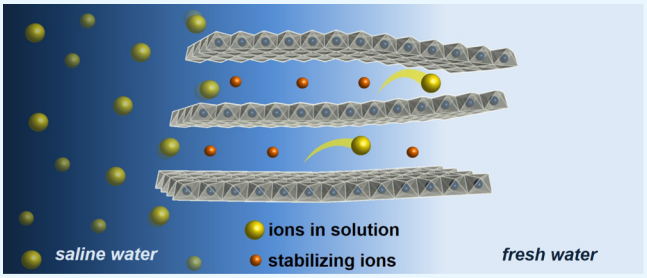

KEYWORDS: *layered manganese oxides, Na-birnessite MnO_2, Mg-buserite MnO_2, hybrid capacitive deionization (HCDI), water desalination, electrochemically induced phase transformation*

1. INTRODUCTION

Estimates place 3.4 billion people at risk of water security; furthermore, climate change, population growth, and industrial development will continue to exacerbate water resources.[1] Liquid surface freshwater constitutes only ∼0.5% of the water available on Earth, and thus purification of brackish and saline water is becoming increasingly important as the water crisis escalates. Reverse osmosis and multistage flash distillation are common methods to remove ions from water, but they are inherently energy demanding.[2] An emerging alternative method, capacitive deionization (CDI), reversibly operates at room temperature and low voltages thus requiring less energy compared to other desalination techniques.[3]

A major limitation in utilizing carbon-based electrodes in CDI devices is relatively low ion adsorption capacity of the materials, which imposes restrictions on the salinity of the feed solution that can be desalinated efficiently to that of brackish water.[4] The ion removal capacity of carbon-based electrodes is limited by the surface area of the materials since ions removed from a solution are stored on carbon surface in the electric double layer.[3,4] One approach to improve ion removal performance is to design electrode materials with chemical and pore structures specifically tuned for efficient desalination of solutions.[5,6] However, by utilizing materials that can remove ions from water via a mechanism that involves interactions with material volume, it is possible to increase the ion-removal capacity of the electrodes further.[4,7−9]

Intercalation host compounds that undergo reversible redox reactions with ions in solutions are a promising class of materials for CDI electrodes. These materials commonly remove ions from the solution through not only surface absorption but also charge transfer and intercalation of the ions into their crystal structure, thereby significantly increasing the ion removal capacity of electrodes. Further, pairing an intercalation electrode that removes cations from a solution, with a carbon electrode that removes anions in a configuration termed hybrid CDI (HCDI) was shown to deliver high ion removal capacity while maintaining high ion removal rates.[7]

Received: June 10, 2018
Accepted: September 5, 2018
Published: September 5, 2018

DOI: 10.1021/acsami.8b09638
ACS Appl. Mater. Interfaces 2018, 10, 32313−32322

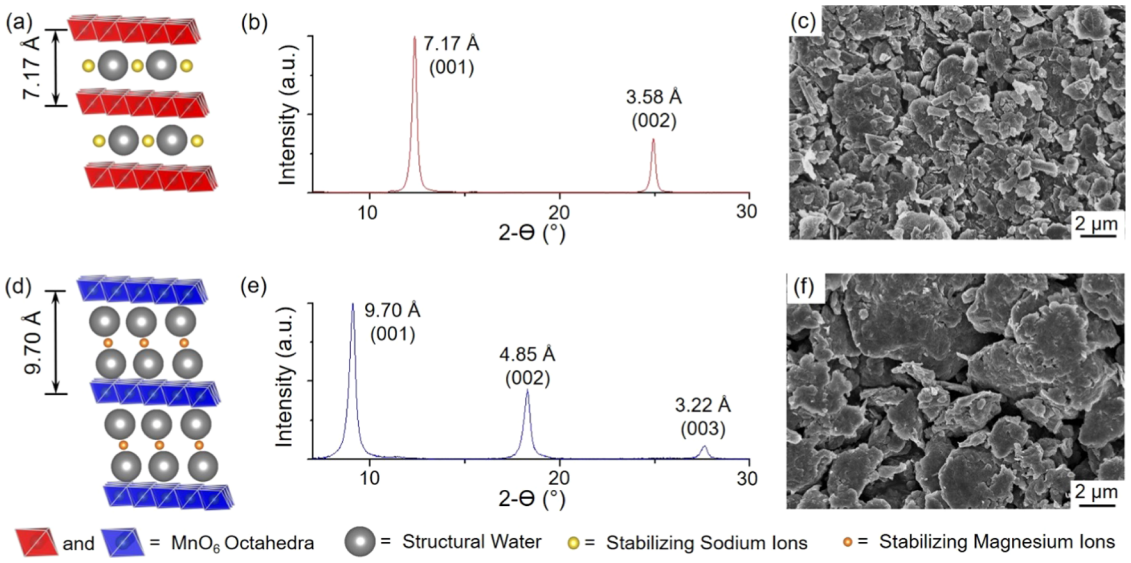

Figure 1. Structure and morphology characterization of the layered manganese oxides. (a) Schematic illustration of the crystal structure, (b) X-ray diffraction (XRD) pattern, and (c) scanning electron microscopy (SEM) image of pristine Na-birnessite powder. (d) Schematic illustration of the crystal structure, (e) XRD pattern, and (f) SEM image of pristine Mg-buserite powder. Red and blue colors are used to visually distinguish data for Na-birnessite and Mg-buserite, respectively.

The selection of redox-active materials for HCDI electrodes is often inspired by the highly developed energy storage field.[4] Computational predictions and experiments have shown that ion intercalation compounds can be used as efficient and reversible electrodes for water desalination.[8−16] However, most studies are commonly carried out in NaCl solution only, whereas the compositions of brackish and ocean water are much more chemically complex. Within the wide library of materials known to be active in electrochemical systems, manganese oxides are especially attractive for application as HCDI electrodes because they are low in cost, environmentally friendly, and show cathodic reduction potentials.[17,18] Previous studies of manganese oxides as HCDI electrodes have involved tunnel manganese oxides (TuMOs)[7,19] and amorphous manganese oxide deposited on carbon support.[20,21] TuMOs with four distinct crystal structures displaying a controlled variation of tunnel size and shape exhibited high performance toward reversible desalination of Na^+, K^+, and Mg^{2+} ions in the HCDI system.[19] Analysis of the mechanism of ion removal revealed contributions of both surface redox reactions and intercalation of ions from solutions into the structural tunnels. It was found that the moderate ability of the α-MnO_2 phase, which contains smaller structural tunnels, to remove larger hydrated Mg^{2+} ions can be overcome by increasing the tunnel size.[19]

Further advancement in CDI performance of the redox-active manganese oxide electrodes can be achieved through utilization of materials with more open structures that have a potential to increase intercalation contribution and achieve higher ion adsorption capacities. Examples of such materials are two-dimensional layered compounds with expanded interlayer spacing that allows for facile insertion and extraction of ions.[22] Indeed, there have been several reports on intercalation host compounds with layered crystal structures, such as transition metal oxides, carbides and sulfides, which showed promising performance in CDI application.[10,23−28] However, none of these layered compounds showed substantially higher gravimetric capacities than those of TuMOs, when normalized by the total mass of electrodes in the HCDI cell,[7,19] triggering interest in investigating CDI performance of the layered manganese oxides (LMOs), which have the advantages of both manganese oxides and layered compounds.

Layered manganese oxides (LMOs) are a class of materials built by the atomic layers of MnO_6 octahedra and stabilized by hydrated cations in the interlayer region that determine the interlayer spacing.[29] LMOs have shown promising performance in charge-storage applications, demonstrating higher reversible capacities and enhanced diffusion of charge-carrying ions compared to TuMO phases.[30−32] Therefore, it is of significant interest to investigate performance of LMOs in HCDI. However, to date there is only a single report on a manganese oxide with a layered crystal structure stabilized by K^+ ions, K-birnessite, in which the authors showed stable cycling performance at modest overall capacity due to the inverted configuration of the electrodes.[18] Key questions about LMOs in a standard HCDI configuration, such as their stability over extended cycling and the relationship between the crystal structure/chemical composition and ion removal performance in solutions containing different salts (i.e., NaCl vs $MgCl_2$), remain unanswered. Moreover, the dynamics of the stabilizing ions in the interlayer region during operation of the HCDI system is unknown.

In this work, two crystallographically and chemically distinct LMO phases, Na-birnessite and Mg-buserite (Figure 1), were investigated as intercalation electrodes for HCDI. The crystal structures of the two LMOs are shown in Figure 1a,d. The layers consist of edge sharing MnO_6 octahedra, whereas Na^+ and Mg^{2+} ions, known as stabilizing ions, occupy the interlayer positions in the Na-birnessite and Mg-buserite, respectively, along with water molecules.[29,33,34] The large difference in interlayer spacing of Na-birnessite (7.2 Å) and Mg-buserite (9.7 Å) is attributed to the different amount of structural water residing between the layers: one layer of water in Na-birnessite compared to two layers of water in Mg-buserite (Figure 1a,d). To understand the ion removal performance of these two

DOI: 10.1021/acsami.8b09638
ACS Appl. Mater. Interfaces 2018, 10, 32313−32322

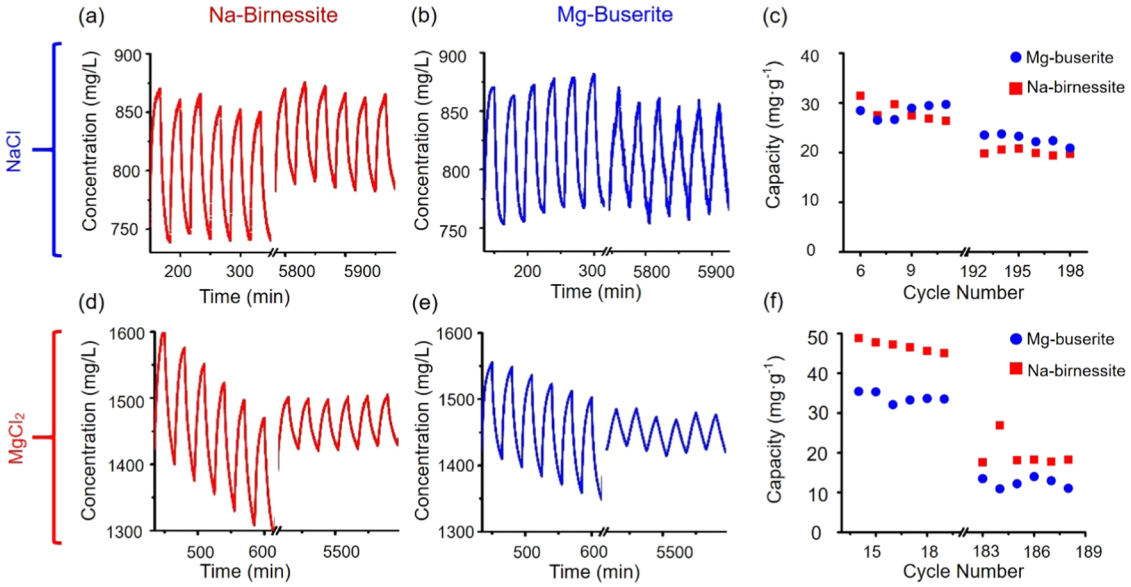

Figure 2. Electrochemical performance of Na-birnessite (red) and Mg-buserite (blue) electrodes in HCDI cells with NaCl and $MgCl_2$ solutions. (a, b, d, e) Concentration vs time plots for (a) Na-birnessite in NaCl solution, cycles 6−12 and 193−198; (b) Mg-buserite in NaCl solution, cycles 6−12 and 193−198; (d) Na-birnessite in $MgCl_2$ solution, cycles 14−19 and 183−188; (e) Mg-buserite in $MgCl_2$ solution, cycles 14−19 and 183−188. (c, f) Ion adsorption capacities (in mg g^{-1}) vs cycle number graphs for both materials in (c) NaCl and (f) $MgCl_2$ solutions.

materials, Na-birnessite and Mg-buserite electrodes were cycled in NaCl and $MgCl_2$ solutions in an electrochemical cell with the HCDI configuration.[19] It is important to study removal of Na^+ and Mg^{2+} ions because they are the first and second most abundant cations present in typical brackish water, respectively.[35] Further, magnesium is a scale-forming element that causes costly buildup in household appliances or cooling towers.[3] The chosen electrode materials and solutions provide a platform to investigate ion dynamics when stabilizing ions in the electrode structure and ions in solution are the same and when they are different. Although it may be ideal to develop materials that can desalinate solutions containing multiple types of ions, here we focus on single salt solutions to understand the fundamental performance of the electrode materials. To gain insights into the stability of layered manganese oxides as HCDI electrodes, the cells were stopped after both 200th ion adsorption step (IAS) and ion release step (IRS), followed by postmortem analysis of the electrode materials structure and composition. Replacing carbon electrode after 200 cycles with a fresh one, allowed us to evaluate the contributions of capacity decay related to the structural changes in layered manganese oxides and oxidation of carbon during cycling.

2. MATERIALS AND METHODS

2.1. Materials Synthesis. Na-birnessite was prepared via mixing a 200 mL solution of 0.6 M NaOH (Acros Organics) and 2.0 M H_2O_2 (Fisher Scientific) with a 100 mL solution of 0.3 M $Mn(NO_3)_2{\cdot}6H_2O$ (Alfa Aesar), following a previously reported procedure.[36] A black precipitate, formed after mixing, was statically aged for 60 h and then filtered and washed until the pH of the filtrate reached ∼10. Washed powder (80 mg) was added to 11.5 mL of 2.0 M NaOH solution in a 23 mL Teflon-lined stainless steel autoclave (Parr Instruments) and hydrothermally treated at 170 °C for 20 h. The product, Na-birnessite, was filtered, washed with deionized water, and dried at 100 °C for 12 h in air.

Mg-buserite was synthesized from the Na-stabilized layered manganese oxide precursor, prepared following a procedure similar to the one described above. Here, the black precipitate was statically aged for 100 h, followed by filtering and washing until the pH of the filtrate reached ∼10. Mg-buserite was formed via ion-exchange process,[37] in which the filtered powder was held in 400 mL of 1.0 M $MgCl_2{\cdot}4H_2O$ (Sigma-Aldrich) solution under stirring for 24 h. The powder was then filtered out, placed in a fresh 400 mL of 1.0 M $MgCl_2$ solution, and stirred for 24 h. The solution replacement process was repeated again for a total of three ion-exchange steps. The product, Mg-buserite powder, was then filtered, washed with deionized water, and dried at 37 °C for 12 h in air. The lower temperature of drying, compared to that used in case of Na-birnessite synthesis, was used to avoid removal of stabilizing water molecules from the interlayer region of Mg-buserite, which can lead to structural transformation.

2.2. Material Characterization. Phase analysis was carried out using a Rigaku Smartlab X-ray diffractometer (XRD) operated at 44 kV and 40 mA with Cu Kα (λ = 1.54056 Å) radiation and a nickel Kβ filter. All scans were performed in a step mode with a 0.02 Å step size and step speed of 6 s. Scanning electron microscope (SEM) images of the electrodes were obtained using a Zeiss Supra 50 VP microscope with an energy dispersive X-ray (EDX) spectroscopy attachment for evaluating the chemical composition of the electrodes before and after cycling. Prior to postmortem SEM/EDX characterization, electrodes removed from the HCDI cell after ion adsorption and ion release steps were thoroughly washed in deionized water and dried at 37 °C. EDX spectra were recorded in 1 μm by 1 μm regions in the center of the electrode film, and Na/Mn and Mg/Mn ratios were determined by averaging the results of three spectra taken from different regions within each electrode. Fourier transform infrared (FTIR) spectra were recorded from activated carbon electrode films using a Perkin Elmer Spectrum One FTIR Spectrometer with KBr as the background.

2.3. Electrode Fabrication. The synthesized Na-birnessite and Mg-buserite powders were utilized as active cathode materials, whereas YP-50 activated carbon (Kuraray Chemical Co., Japan) served as the active anode material. Electrodes were prepared by mixing active materials with carbon black (Alfa Aesar) and poly(tetrafluoroethylene) (PTFE) (Sigma-Aldrich) binder in a weight ratio of 80:15:5 in ethanol. The resulting paste was then rolled into electrode films, and the thickness of the anode and cathode films were 300 and 150 μm, respectively. The carbon anodes were thicker than the manganese oxide cathodes to compensate for lower surface-based ion adsorption capacity of the carbon. After fabrication, the Na-birnessite and carbon electrodes were dried at 100 °C for 1 h. The

DOI: 10.1021/acsami.8b09638
ACS Appl. Mater. Interfaces 2018, 10, 32313−32322

Mg-buserite electrodes were dried at 37 °C for 3 h to avoid thermal decomposition of the Mg-buserite phase that occurs at ~70 °C.[38]

2.4. Electrochemical Desalination Experiments. Electrochemical characterization was performed using a custom-build HCDI cell integrated with a Biologice VMP3 potentiostat and a peristaltic pump operated at 20 mL min^{-1} flow rate in a batch mode (Figure S1), as described previously.[19] In short, tin-coated current collectors (3M), nylon mesh spacers (Spectrum Laboratories, Inc.), Viton fluoroelastomer gasket (500 μm thickness, McMasterCarr) with a precut flow channel (area of flow channel = 294 mm^2), LMO and carbon electrodes, and both anion and cation ion-exchange membranes (AMV, Selemion, AGC engineering Co.) were used in the cell. For all tests, five precycles with a 5 min half-step length were performed to reach a dynamic steady state condition.[39] This was followed by normal cycling with 15 min ion adsorption and 15 min ion release cycles at applied potentials of 1.2 and −1.2 V, respectively. The term "ion adsorption" refers to the step in which ions are removed from solutions to be consistent with nomenclature used in the CDI community, but does not represent the mechanism by which the ions are removed from solutions. A dip-in conductivity probe with a conductivity isopod (EY915, eDAQ Pty Ltd, Australia) was paired to measure conductivity of the test solution vs time. Conductivities of the NaCl and $MgCl_2$ solutions were converted to concentration based on previously reported relationships.[19] The starting solution concentration was 15 mM for both NaCl and $MgCl_2$ solutions.

The following eq 1 was used to calculate ion adsorption capacity in the HCDI cell

$$\text{capacity} = \frac{\Delta C \times V}{M} \quad (1)$$

where ΔC is the absolute difference between the maximum and minimum of concentration (mg L^{-1}) during each respective cycle, V is the volume of a solution (L), and M is the total mass of the electrodes exposed in the flow channel (g), including the masses of the conductive and binder additives. This method of ion removal capacity calculation is commonly utilized in the CDI community.[3]

3. RESULTS AND DISCUSSION

Figure 1 shows structure and morphology characterization of pristine Na-birnessite (Figure 1a−c) and Mg-buserite (Figure 1d−f) powders. The XRD pattern of the synthesized Na-birnessite (Figure 1b) can be indexed to JCPDS #23-1046, and EDX spectroscopy data (Figure S2a, Supporting Information) confirms the presence of sodium in material composition, so that its formula can be estimated as $Na_{0.28}MnO_2$. The XRD pattern of the Mg-buserite (Figure 1e) agrees well to JCPDS #32-1128. Analysis of the EDX spectrum (Figure S2b, Supporting Information) revealed that the chemical composition of this phase can be estimated as $Mg_{0.14}MnO_2$. The interlayer spacings, d, calculated from the positions of (001) reflections in the XRD patterns are consistent with the previously reported data for LMOs: d = 7.17 Å for Na-birnessite and d = 9.70 Å for Mg-buserite.[33] SEM images in Figure 1c,f, show that both materials have a platelet morphology with similar lateral size of the particles of 1−2 μm, forming larger multiparticle flakes.

Table 1. Maximum Ion Removal Capacities Exhibited by Na-Birnessite and Mg-Buserite Electrodes in NaCl and $MgCl_2$ Solutions

	maximum capacity (mg g^{-1})	maximum capacity (μmol g^{-1})
	NaCl Solution	
Na-birnessite	31.5	539
Mg-buserite	37.2	637
	$MgCl_2$ Solution	
Na-birnessite	50.2	527
Mg-buserite	39.0	410

Interactions between LMO electrodes and Na^+ or Mg^{2+} ions in solution were studied via extended cycling in the custom-built HCDI cell.[19] Both Na-birnessite and Mg-buserite electrodes exhibited highly reversible behavior of ion adsorption/ion release in NaCl and $MgCl_2$ solutions (Figure 2). Figure 2a−c shows the concentration vs time profiles and ion adsorption capacity vs cycle number data for both electrodes in NaCl solution. Maximum Na^+ ion removal capacities of 31.5 and 37.2 mg g^{-1} were delivered by the Na-birnessite and Mg-buserite, respectively, within the first 10 cycles (Table 1). Figure 2d−f shows the same electrochemical data for both materials in $MgCl_2$ solution. The maximum Mg^{2+} ion removal capacities of the Na-birnessite and Mg-buserite electrodes, exhibited within the first 10 cycles, were 50.2 and 39.0 mg g^{-1}, respectively.

Although in case of reports discussing performance of the HCDI systems solely in NaCl solution, it is common to report ion adsorption capacity in terms of mg of salt per gram of electrode, to accurately compare performance of electrode materials in two different solutions containing salts with different molar masses, the ion adsorption capacities must be normalized by the molar mass of the salt (NaCl or $MgCl_2$) and presented as values with units of μmol g^{-1}.[3] Therefore the maximum ion adsorption capacities are shown as values in both mg and μmol of salt per gram of electrode in Table 1. A previous report on TuMOs showed that the ion removal capacity of the manganese oxides correlated well to the radius of hydrated cations removed from solutions.[19] A similar trend is found here, with both LMO phases removing a greater amount of NaCl, than $MgCl_2$, from the solution (Table 1), which is attributed to the smaller radius of the hydrated Na^+ ions compared to that of Mg^{2+} ions.[40] In NaCl solution, Mg-buserite demonstrated a larger capacity than Na-birnessite (Table 1), which could be ascribed to the larger interlayer spacing in Mg-buserite allowing for a greater amount of Na^+ ions to be inserted. Interestingly, in $MgCl_2$ solution, Na-birnessite demonstrated a higher capacity (Table 1). This experimental observation cannot be easily explained, and further study is necessary to understand this phenomenon.

Extended applications of Na-birnessite and Mg-buserite phases as HCDI electrodes for 200 ion adsorption/ion release cycles in both NaCl and $MgCl_2$ solutions revealed that cells with both electrodes demonstrated gradual decrease of ion adsorption capacity (Figure 2). Both materials demonstrated a better capacity retention in NaCl solution than in $MgCl_2$ solution, likely due to the more facile diffusion of the singly charged Na^+ ions, compared to doubly charged Mg^{2+} ions, in the interlayer region of LMO structure.[41] To better understand the mechanism of capacity fade, morphological, compositional, and structural changes in the electrodes were characterized ex situ via SEM, EDX, and XRD analyses.

SEM images of the pristine and cycled electrodes shown in Figure S3 (Supporting Information) showed no significant morphological changes after 200 ion adsorption/ion release cycles, with the characteristic platelet morphology of active materials remaining in all cycled electrodes. However, there were distinct changes in both the chemical composition and interlayer spacing after ion removal experiments in both NaCl and $MgCl_2$ solutions.

DOI: 10.1021/acsami.8b09638
ACS Appl. Mater. Interfaces 2018, 10, 32313−32322

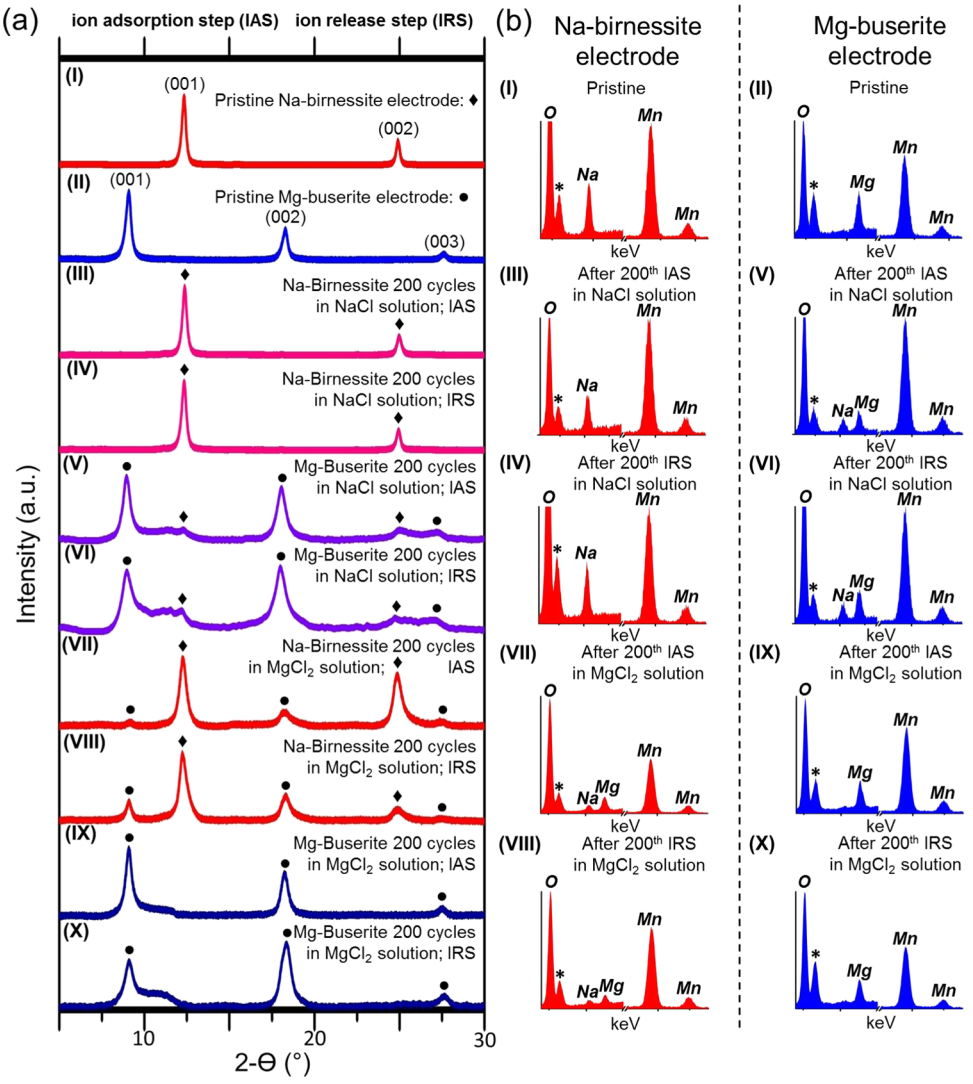

Figure 3. Characterization of the structural and compositional modifications of Na-birnessite and Mg-buserite electrodes over extended cycling in the HCDI cells in NaCl or $MgCl_2$ solutions. (a) XRD patterns and (b) EDX spectra of the following electrodes: (I) pristine Na-birnessite; (II) pristine Mg-buserite; (III, IV) Na-birnessite cycled for 200 cycles in NaCl solution and stopped after (III) ion adsorption step and (IV) ion release step; (V, VI) Mg-buserite cycled for 200 cycles in NaCl solution and stopped after (V) ion adsorption step and (VI) ion release step; (VII, VIII) Na-birnessite cycled for 200 cycles in $MgCl_2$ solution and stopped after (VII) ion adsorption step and (VIII) ion release step; (IX, X) Mg-buserite cycled for 200 cycles in $MgCl_2$ solution and stopped after (IX) ion adsorption step and (X) ion release step. *indicates fluorine peak from the PTFE binder used for the electrodes fabrication.

Table 2. Na/Mn and Mg/Mn Ratios in Na-Birnessite and Mg-Buserite Electrodes before and after 200 Cycles in NaCl and $MgCl_2$ Solutions

Testing conditions	Na/Mn	Mg/Mn
Pristine Na-birnessite electrode (I)[a]	0.28	0.00
Pristine Mg-buserite electrode (II)[a]	0.00	0.14
Na-birnessite electrode after 200th IAS in NaCl solution (III)[a]	0.24	0.00
Na-birnessite electrode after 200th IRS in NaCl solution (IV)[a]	0.18	0.00
Mg-buserite electrode after 200th IAS in NaCl solution (V)[a]	0.19	0.16
Mg-buserite electrode after 200th IRS in NaCl solution (VI)[a]	0.13	0.05
Na-birnessite electrode after 200th IAS in $MgCl_2$ solution (VII)[a]	0.09	0.27
Na-birnessite electrode after 200th IRS in $MgCl_2$ solution (VIII)[a]	0.07	0.10
Mg-buserite electrode after 200th IAS in $MgCl_2$ solution (IX)[a]	0.00	0.32
Mg-buserite electrode after 200th IRS in $MgCl_2$ solution (X)[a]	0.00	0.13

[a]The Roman numbers in parentheses (I–X) indicate the same electrodes for which XRD patterns and SEM images are shown in Figures 3 and S3, respectively.

DOI: 10.1021/acsami.8b09638
ACS Appl. Mater. Interfaces 2018, 10, 32313–32322

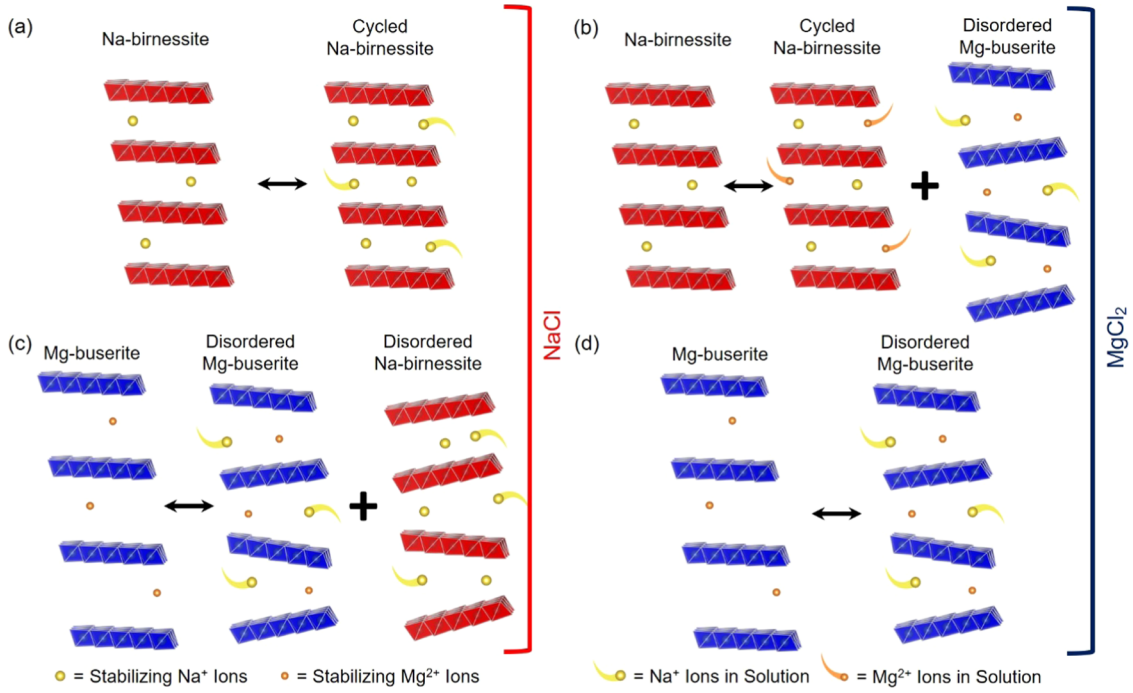

Figure 4. Schematic illustration of the Na-birnessite (red) and Mg-buserite (blue) crystal structures before and after cycling in (a, c) NaCl and (b, d) $MgCl_2$ solutions. (a) Na-birnessite electrode before and after cycling in NaCl solution demonstrating minor structural change; (b) Na-birnessite electrode before and after cycling in $MgCl_2$ solution indicating partial transformation into disordered Mg-buserite phase; remaining Na-birnessite structure exhibited minor structural change; (c) Mg-buserite electrode before and after cycling in NaCl solution indicating transformation into disordered Mg-buserite phase and disordered Na-birnessite phase; (d) Mg-buserite electrode after cycling in $MgCl_2$ solution showing increasing structural disorder.

The chemical composition of the thoroughly washed cycled electrodes was determined via analysis of EDX spectroscopy data (Figure 3 and Table 2) and revealed decrease in both stabilizing ion and ion from solution content after the 200th ion release step (IRS) compared to that after the 200th ion adsorption step (IAS). This confirms that LMO electrodes removed cations from solution not only through surface adsorption but also via redox reactions with the electrode materials, similarly to tunnel manganese oxides.[19] In case of the electrodes cycled in solutions containing ions other than stabilizing ions (e.g., Mg-buserite in NaCl solution), the EDX spectroscopy data revealed presence of the ions from solution in the composition of layered manganese oxides (Table 2).

When tested in solutions containing the same cations as stabilizing cations, Na-birnessite and Mg-buserite exhibit distinctly different structural dynamics. In case of the Na-birnessite electrode cycled in NaCl solution, the diffraction patterns of the electrodes after 200 cycles (Figure 3a-III,IV) show no significant changes compared to the XRD pattern of the pristine electrode (Figure 3a-I), indicating excellent structural stability of Na-birnessite in a solution with no foreign cation present. However, the XRD patterns of the cycled Mg-buserite electrode clearly show a shoulder to the right of the (001) peak after both 200th IAS and 200th IRS (Figure 3a-IX,X), which is not present in the diffraction pattern of the pristine electrode (Figure 3a-II). The presence of the shoulder is accompanied by the change in intensity ratio of the (001) and (002) peaks. These changes in the XRD patterns of the Mg-buserite electrode indicate that the material undergoes increasing structural disorder with cycling. Expanded interlayer spacing in the Mg-buserite structure allows for facile mobility of ion in/from the interlayer region, supported by large changes in Mg/Mn ratio between 200th IAS and IRS (Table 2). When ions are extracted from the interlayer region, the Mn−O layers lose rigidity and lamellar ordering, leading to the change in intensities of the peaks and appearance of the shoulder in the XRD pattern.

Similar phenomena were observed in case of Mg-buserite electrode cycled in NaCl solution. Both XRD patterns obtained after 200th IAS and 200th IRS (Figure 3a-V,VI) exhibited a shoulder at angles higher than that of (001) peak, indicating disorder in lamellar stacking of the Mn−O layers, whereas change in the ratio of intensities of (001) and (002) peaks pointed at structural disorder within Mn−O layers. Moreover, the XRD pattern of the Mg-buserite electrode cycled in NaCl solution for 200 cycles showed peaks at 12.4 and 24.9° 2θ corresponding to the (001) and (002) reflections of the interplane distance of ~7 Å. This distance matches the interlayer spacing in the Na-birnessite phase. In addition, the EDX spectroscopy measurements clearly showed presence of both sodium and magnesium in the chemical composition of the cycled electrode after 200th IAS and 200th IRS (Figure 3b-V,VI; Table 2). These results indicate that when the Mg-buserite electrode was cycled in NaCl solution, Na^+ ions were inserted into the Mg-buserite structure during each IAS. During IRS, fractions of the inserted Na^+ ions and stabilizing Mg^{2+} ions were extracted from the interlayer region simultaneously, resulting in gradual change in chemical composition and structure of the active electrode material. These structural and compositional modifications led to the decreased interlayer spacing in the Mg-buserite electrodes after cycling in NaCl solution, due to the smaller radius of hydrated Na^+ ions compared to that of hydrated Mg^{2+} ions.

DOI: 10.1021/acsami.8b09638
ACS Appl. Mater. Interfaces 2018, 10, 32313−32322

Table 3. Ion Removal Capacities of Intercalation Electrodes with Layered Crystal Structures Cycled in Cells with the HCDI Configuration in NaCl Solution

Material	Current/Voltage	Exchange membranes	Solution strength (mM)	Flow rate (mL min^{-1})	Capacity (mg g^{-1})	Capacity retention (% after N cycles)	Ref
TiS_2–CNT	constant 100 mA g^{-1} current to 0.8 V, held 60 min desorb 0.2 V	none	50	22	12.6	~100% after 70 cycles	27
MWCNT–hV_2O_5	constant 33 mA g^{-1} current to 0.8 V, held 60 min desorb −0.4 V	anion and cation	200	5	~26	85% after 100 cycles	24
exfoliated MoS_2	1.2–0 V (75 min)	none	50	NR	4.41	NR	43
K-birnessite	1.0–0 V (5 min)	none	8.6	9.2	14.9	95.4% after 350 cycles	28
Na-birnessite	1.2 to −1.2 V (15 min)	anion and cation	15	20	31.5	66% after 200 cycles	this work
Mg-buserite	1.2 to −1.2 V (15 min)	anion and cation	15	20	37.2	75% after 200 cycles	this work

In case of the Na-birnessite electrode cycled in $MgCl_2$ solution, analysis of the chemical composition (Figure 3b-VII,VIII; Table 2) after 200 cycles revealed presence of magnesium in the structure of the material. Additionally, the XRD patterns clearly showed peaks at 9.1, 18.3, and 27.6° (Figure 3a-VII,VIII) corresponding to the interlayer distance of ~10 Å matching the interlayer spacing of the Mg-buserite phase. Therefore, it is evident that Mg-buserite forms during extended cycling of Na-birnessite electrode in $MgCl_2$ solution. The phase transformation is likely to occur due to the insertion of the hydrated Mg^{2+} ions into the interlayer region during IAS, leading to the increased interlayer spacing, and not all of these Mg^{2+} ions are released during IRS. Simultaneously, during the IRS, a fraction of the stabilizing Na^+ ions is extracted from the interlayer region of the Na-birnessite phase (Table 2). Over continued cycling, this phenomenon results in the interlayer content changing to reflect the chemical composition of the solution being desalinated and the observed formation of LMO phases with altered interlayer spacing. The intensities of the peaks corresponding to the Mg-buserite phase in case of Na-birnessite electrode cycled in $MgCl_2$ solution are relatively low (Figure 3a-VII,VIII), making it difficult to clearly see the presence of the shoulders next to the peaks. However, based on the relative peak intensities ratio of the peaks corresponding to the Mg-buserite phase, as well as the peaks in the XRD pattern of the Mg-buserite electrode cycled in $MgCl_2$ solution containing shoulders (Figure 3a-IX,X), we believe that Mg-buserite phase forming in the process of cycling of Na-birnessite electrode in $MgCl_2$ solution is a disordered phase, similar to that forming in case of cycling of Mg-buserite electrode in $MgCl_2$ solution.

The structural evolution of Na-birnessite and Mg-buserite electrodes occurring in the process of extended reversible cycling in NaCl and $MgCl_2$ solutions is schematically depicted in Figure 4. In case of solutions containing ions other than stabilizing ions, both materials undergo electrochemically induced phase transformation with extended application as HCDI electrodes due the change in interlayer cation content, observed via EDX spectroscopy. Analysis of the XRD patterns revealed that structural disorder was more pronounced in case of Mg-buserite electrodes after cycling, whereas Na-birnessite electrodes showed better structural stability, especially in NaCl solution. This stable behavior can be attributed to the higher crystallinity of the pristine Na-birnessite phase relative to the pristine Mg-buserite phase, as evident from the full width at half maximum value of the (001) peaks in the XRD patterns of both materials (Figure S4, Supporting Information).[42] Notably, after IAS in case of Na-birnessite electrode cycled in $MgCl_2$ solution, the relative height of the (002) peak increases relative to the pristine electrode, but after IRS the relative height returns to a similar value as that in the XRD pattern of the pristine material. This observation indicates that when larger Mg^{2+} ions are inserted in Na-birnessite, the structure undergoes some disorder, and when they are released, the structure returns to the similar order as in the pristine electrode. Therefore, utilizing LMOs with high crystallinity as active materials in HCDI electrodes is a promising strategy that can lead to enhanced structural and thus electrochemical stability of the electrodes after extended cycling.

Our results show that the interlayer content in LMO phases gradually changes as electrodes undergo multiple ion adsorption/ion release steps in the HCDI cell. A similar

DOI: 10.1021/acsami.8b09638
ACS Appl. Mater. Interfaces 2018, 10, 32313−32322

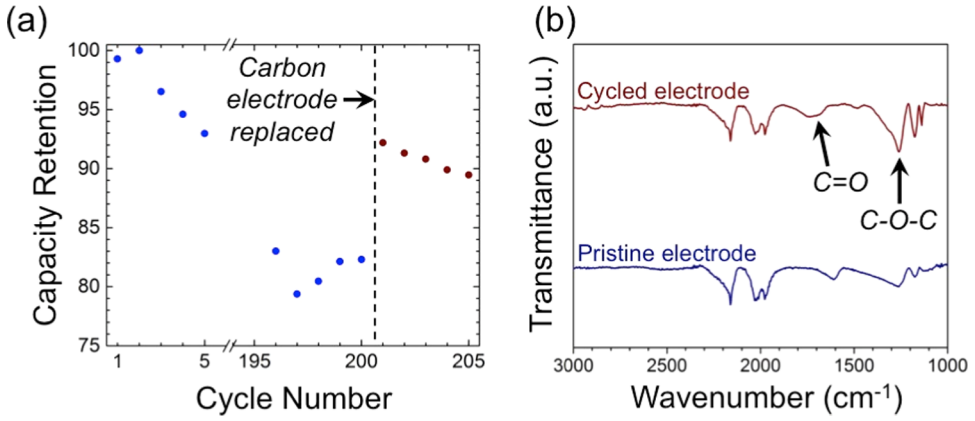

Figure 5. (a) Capacity retention (normalized by maximum ion removal capacity) of the HCDI cell containing Mg-buserite and activated carbon electrodes in NaCl solution shown before and after replacement of carbon electrode. (b) FTIR spectra recorded from the pristine activated carbon electrode and activated carbon electrode removed from the HCDI cell after 200 cycles.

phenomenon was reported for the K-birnessite electrode operated under inverted HCDI testing conditions in NaCl solution, where K^+ ions were gradually replaced by Na^+ ions during cycling.[28] Hence, we believe that the change in the chemical composition of the interlayer species, including the release of the stabilizing ions and incorporation of the ions from the solution, is likely to occur in most layered oxides and possibly other families of the layered compounds used in electrochemical water desalination. This finding is important as it clearly shows that the interlayer content and thus the interlayer spacing change based on the composition of the solution being desalinated, which can potentially lead to changes in electrode material properties and performance.

The layered manganese oxides, stabilized by Na^+ and Mg^{2+} ions, presented here demonstrate high ion removal capacities in NaCl and $MgCl_2$ solutions. The ion removal capacities exhibited by Na-birnessite and Mg-buserite compare favorably with those reported in the past for redox-active intercalation host compounds with layered crystal structures versus carbon electrodes in an HCDI configuration in NaCl solution (Table 3). Similar benchmarks for the removal of Mg^{2+} ions cannot be provided as reports on desalinating solutions of ions beyond Na^+ ions are still not common. The LMOs exhibited markedly higher maximum ion removal capacities toward removal of Na^+ ions than previously reported layered oxides and sulfides in HCDI configurations.[24,27,28,43] Although factors, such as inclusion of ion exchange membranes, applied potential and duration of the IAS/IRS, can affect performance, our results demonstrate the promise of the low-cost and environmentally friendly LMOs as high capacity electrodes for electrochemical water desalination.

The high initial ion removal capacity of both Na-birnessite and Mg-buserite electrodes, however, substantially declined over the course of 200 ion adsorption/ion release cycles (Table 3). Given that the structural evolution of the electrodes involves only transformations between two LMO phases under study, both of which are highly active initially, and increasing disorder of lamellar stacking, such performance decay is unexpectedly rapid. It was reported previously, though, that similar phenomenon in the CDI cell was attributed to the oxidation of the counter carbon electrode.[44] To exclude the effect of the carbon electrode oxidation on capacity fade and understand the stability of the LMOs themselves, an HCDI cell containing Mg-buserite electrode was cycled for 200 cycles in NaCl solution (during which the capacity dropped to 82% of the initial value, Figure 5a) removed from the cell, and used in a new HCDI cell assembled with a fresh carbon electrode. This new cell was cycled again in NaCl solution. It was found that the ion adsorption capacity of Mg-buserite electrode returned to 92% of its initial value after replacing the carbon electrode (Figure 5a). Further, analysis of the FTIR spectra shown in Figure 5b confirmed oxidation of the cycled carbon electrode, with bands at 1733 and 1260 cm^{-1} present in the spectra from the electrode that was cycled 200 times. These bands can be attributed to C═O and C−O−C vibrations, respectively.[45,46] This finding indicates that the deterioration of the HCDI cell performance can be to the large extent attributed to the oxidation of carbon electrode and highlights the importance of controlling cycling parameters, such as the potential window, duration of steps, etc., to prevent oxidation of carbon. Utilization of such strategies was recently shown to result in stable cycling performance, though at low capacity values.[28] Therefore, a tradeoff between the stability and ion adsorption capacity exists and needs to be investigated further. The return of the ion adsorption capacity to 92% of its initial value shown here demonstrates the high potential of LMOs in extended HCDI cycling. The ion removal capacity decay of 8% over 200 cycles can be attributed to the structural changes of Mg-buserite phase and can be minimized by controlling crystallinity of the material as discussed above.

The changes in interlayer content and interlayer spacing induced by extended cycling in HCDI approach are important factors to consider for prolonged application of LMO electrodes. Although oxidation of carbon electrode was identified as the main contributor to capacity fade in the HCDI cell in this work, the LMO electrodes also contribute to the capacity decay over 200 cycles. Enhanced stability of the materials with layered crystal structures for extended HCDI electrode application could be achieved through inserting pillaring ions/molecules, similarly to the battery electrode materials,[47] fabrication of two-dimensional heterostructured electrodes,[48] formation of hybrid electrodes with materials having superior electronic conductivity (e.g., graphene),[5,49] or through stabilization of electrodes with carbon nanotubes, which was shown to be effective in providing enhanced electrical conductivity and/or physical structure stability for molybdenum disulfide, molybdenum carbide, and titanium disulfide in CDI and HCDI configurations.[25−27] The high

DOI: 10.1021/acsami.8b09638
ACS Appl. Mater. Interfaces 2018, 10, 32313−32322

capacity and low cost of LMOs, combined with a potential to improve their stability, make them promising candidates for application in not only HCDI but also other water desalination configurations, such as desalination batteries.

4. CONCLUSIONS

Manganese oxides with layered crystal structure stabilized by Na^+ (Na-birnessite) and Mg^{2+} (Mg-buserite) ions were for the first time evaluated as electrode materials for the removal of Na^+ and Mg^{2+} ion from aqueous solutions in HCDI electrochemical system. Both materials demonstrated high initial ion removal capacities, but gradual capacity fading over the course of 200 ion adsorption/ion release cycles. Analysis of the structure and chemical composition of the cycled electrodes revealed that decay in ion removal performance was caused by oxidation of the carbon electrode and structural disorder of manganese oxide electrodes. Our results indicate that parameters, such as interlayer spacing, stabilizing ions, ions in solution, and crystallinity of materials, all play important roles in defining performance of LMOs during extended cycling in HCDI application. The interlayer spacing and interlayer species of LMOs gradually transform based on the composition of the solution being desalinated. These findings emphasize the need to probe long-term structural and chemical stability of the electrode materials used in CDI approach for water desalination, especially those with open-layered structures favoring intercalation reactions. Understanding of factors contributing to performance decay is critical for developing strategies eliminating their negative effect and creating next-generation electrochemical devices with high performance for water desalination.

■ ASSOCIATED CONTENT

Supporting Information

The Supporting Information is available free of charge on the ACS Publications website at DOI: 10.1021/acsami.8b09638.

Schematic illustration of HCDI cell used for evaluating the ion removal behavior of layered manganese oxide electrodes investigated in this work (Figure S1); EDX spectra of pristine Na-birnessite and Mg-buserite powders (Figure S2); SEM images of the pristine and cycled electrodes (Figure S3); XRD patterns of pristine Na-birnessite and Mg-buserite electrodes with full width at half-maximum values of (001) peak (Figure S4) (PDF)

■ AUTHOR INFORMATION

Corresponding Author

*E-mail: ep423@drexel.edu. Phone: (215)-571-4612.

ORCID

Ekaterina Pomerantseva: 0000-0002-6765-7133

Author Contributions

†B.W.B. and B.H.-O. contributed equally to this work.

Notes

The authors declare no competing financial interest.

■ ACKNOWLEDGMENTS

This work was supported by the National Science Foundation (CMMI-1635233). The authors would like to thank Mallory Clites for assistance with SEM, EDX spectroscopy, and FTIR spectroscopy analysis, as well as the Drexel Centralized Research Facilities for their support with materials characterization.

■ REFERENCES

(1) Vorosmarty, C. J.; McIntyre, P. B.; Gessner, M. O.; Dudgeon, D.; Prusevich, A.; Green, P.; Glidden, S.; Bunn, S. E.; Sullivan, C. A.; Liermann, C. R.; Davies, P. M. Global Threats to Human Water Security and River Biodiversity. *Nature* **2010**, *467*, 555−561.

(2) Youssef, P. G.; Al-Dadah, R. K.; Mahmoud, S. M. Comparative Analysis of Desalination Technologies. *Energy Procedia* **2014**, *61*, 2604−2607.

(3) Suss, M. E.; Porada, S.; Sun, X.; Biesheuvel, P. M.; Yoon, J.; Presser, V. Water Desalination via Capacitive Deionization: What is it and what can we expect from it? *Energy Environ. Sci.* **2015**, *8*, 2296−2319.

(4) Suss, M. E.; Presser, V. Water Desalination with Energy Storage Electrode Materials. *Joule* **2018**, *2*, 10−15.

(5) Ren, Q.; Wang, G.; Wu, T.; He, X.; Wang, J.; Yang, J.; Yu, C.; Qiu, J. Calcined MgAl-layered Double Hydroxide/graphene Hybrids for Capacitive Deionization. *Ind. Eng. Chem. Res.* **2018**, *57*, 6417−6425.

(6) Wang, G.; Qian, B.; Dong, Q.; Yang, J.; Zhao, Z.; Qiu, J. Highly Mesoporous Activated Carbon Electrode for Capacitive Deionization. *Sep. Purif. Technol.* **2013**, *103*, 216−221.

(7) Lee, J.; Kim, S.; Kim, C.; Yoon, J. Hybrid Capacitive Deionization to Enhance the Desalination Performance of Capacitive Techniques. *Energy Environ. Sci.* **2014**, *7*, 3683−3689.

(8) Kim, S.; Lee, J.; Kim, C.; Yoon, J. $Na_2FeP_2O_7$ as a Novel Material for Hybrid Capacitive Deionization. *Electrochim. Acta* **2016**, *203*, 265−271.

(9) Guo, L.; Mo, R.; Shi, W.; Huang, Y.; Leong, Z. Y.; Ding, M.; Chen, F.; Yang, H. Y. A Prussian Blue Anode for High Performance Electrochemical Deionization Promoted by the Faradaic Mechanism. *Nanoscale* **2017**, *9*, 13305−13312.

(10) Srimuk, P.; Kaasik, F.; Kruner, B.; Tolosa, A.; Fleischmann, S.; Jackel, N.; Tekeli, M. C.; Aslan, M.; Suss, M. E.; Presser, V. MXene as a Novel Intercalation-type Pseudocapacitive Cathode and Anode for Capacitive Deionization. *J. Mater. Chem. A* **2016**, *4*, 18265−18271.

(11) Porada, S.; Shrivastava, A.; Bukowska, P.; Biesheuvel, P.; Smith, K. C. Nickel Hexacyanoferrate Electrodes for Continuous Cation Intercalation Desalination of Brackish Water. *Electrochim. Acta* **2017**, *255*, 369−378.

(12) Singh, K.; Bouwmeester, H.; de Smet, L.; Bazant, M.; Biesheuvel, P. Theory of Water Desalination with Intercalation Materials. *Phys. Rev. Appl.* **2018**, *9*, No. 064036.

(13) Shanbhag, S.; Bootwala, Y.; Whitacre, J. F.; Mauter, M. S. Ion Transport and Competition Effects on $NaTi_2(PO_4)_3$ and $Na_4Mn_9O_{18}$ Selective Insertion Electrode Performance. *Langmuir* **2017**, *33*, 12580−12591.

(14) Kim, T.; Yoon, J. CDI Ragone Plot as a Functional Tool to Evaluate Desalination Performance in Capacitive Deionization. *RSC Adv.* **2015**, *5*, 1456−1461.

(15) Liu, S.; Smith, K. C. Quantifying the Trade-offs Between Energy Consumption and Salt Removal Rate in Membrane-free Cation Intercalation Desalination. *Electrochim. Acta* **2018**, *271*, 652−665.

(16) Smith, K. C. Theoretical Evaluation of Electrochemical Cell Architectures using Cation Intercalation Electrodes for Desalination. *Electrochim. Acta* **2017**, *230*, 333−341.

(17) Julien, C. M.; Mauger, A. Nanostructured MnO_2 as Electrode Materials for Energy Storage. *Nanomaterials* **2017**, *7*, No. 396.

(18) Zhang, K.; Han, X.; Hu, Z.; Zhang, X.; Tao, Z.; Chen, J. Nanostructured Mn-based Oxides for Electrochemical Energy Storage and Conversion. *Chem. Soc. Rev.* **2015**, *44*, 699−728.

(19) Byles, B. W.; Cullen, D. A.; More, K. L.; Pomerantseva, E. Tunnel Structured Manganese Oxide Nanowires as Redox Active Electrodes for Hybrid Capacitive Deionization. *Nano Energy* **2018**, *44*, 476−488.

(20) Hand, S.; Cusick, R. D. Characterizing the Impacts of Deposition Techniques on the Performance of MnO_2 Cathodes for Sodium Electrosorption in Hybrid Capacitive Deionization. *Environ. Sci. Technol.* **2017**, *51*, 12027−12034.
(21) Liu, Y.-H.; Hsi, H.-C.; Li, K.-C.; Hou, C.-H. Electrodeposited Manganese Dioxide/Activated Carbon Composite as a High-performance Electrode Material for Capacitive Deionization. *ACS Sustainable Chem. Eng.* **2016**, *4*, 4762−4770.
(22) Pomerantseva, E.; Resini, C.; Kovnir, K.; Kolen'ko, Y. V. Emerging Nanostructured Electrode Materials for Water Electrolysis and Rechargeable Beyond Li-ion Batteries. *Adv. Phys.: X* **2017**, *2*, 211−253.
(23) Bao, W.; Tang, X.; Guo, X.; Choi, S.; Wang, C.; Gogotsi, Y.; Wang, G. Porous Cryo-Dried MXene for Efficient Capacitive Deionization. *Joule* **2018**, *2*, 778−787.
(24) Lee, J.; Srimuk, P.; Aristizabal, K.; Kim, C.; Choudhury, S.; Nah, Y.-C.; Mücklich, F.; Presser, V. Pseudocapacitive Desalination of Brackish Water and Seawater with Vanadium-Pentoxide-Decorated Multiwalled Carbon Nanotubes. *ChemSusChem* **2017**, *10*, 3611−3623.
(25) Srimuk, P.; Halim, J.; Lee, J.; Tao, Q.; Rosen, J.; Presser, V. Two-Dimensional Molybdenum Carbide (MXene) with Divacancy Ordering for Brackish and Seawater Desalination via Cation and Anion Intercalation. *ACS Sustainable Chem. Eng.* **2018**, *6*, 3739−3747.
(26) Srimuk, P.; Lee, J.; Fleischmann, S.; Choudhury, S.; Jackel, N.; Zeiger, M.; Kim, C.; Aslan, M.; Presser, V. Faradaic Deionization of Brackish and Sea Water via Pseudocapacitive Cation and Anion Intercalation into Few-layered Molybdenum Disulfide. *J. Mater. Chem. A* **2017**, *5*, 15640−15649.
(27) Srimuk, P.; Lee, J.; Tolosa, A.; Kim, C.; Aslan, M.; Presser, V. Titanium Disulfide: A Promising Low-Dimensional Electrode Material for Sodium Ion Intercalation for Seawater Desalination. *Chem. Mater.* **2017**, *29*, 9964−9973.
(28) Wu, T.; Wang, G.; Wang, S.; Zhan, F.; Fu, Y.; Qiao, H.; Qiu, J. Highly Stable Hybrid Capacitive Deionization with a MnO_2 Anode and a Positively Charged Cathode. *Environ. Sci. Technol. Lett.* **2018**, *5*, 98−102.
(29) Post, J. E. Manganese Oxide Minerals: Crystal Structures and Economic and Environmental Significance. *Proc. Natl. Acad. Sci. U.S.A.* **1999**, *96*, 3447−3454.
(30) Byles, B. W.; Pomerantseva, E. Reversible Intercalation of Lithium and Sodium Ions into Layered and Tunnel Structured Manganese Oxides: One-Dimensional versus Two-Dimensional Diffusion. In *Low-Dimensional Materials and Devices*, Proceedings of SPIE; International Society for Optics and Photonics, 2017; p 103490G.
(31) Ghodbane, O.; Ataherian, F.; Wu, N.-L.; Favier, F. In situ Crystallographic Investigations of Charge Storage Mechanisms in MnO_2-based Electrochemical Capacitors. *J. Power Sources* **2012**, *206*, 454−462.
(32) Ghodbane, O.; Pascal, J.-L.; Favier, F. Microstructural Effects on Charge-Storage Properties in MnO_2-based Electrochemical Supercapacitors. *ACS Appl. Mater. Interfaces* **2009**, *1*, 1130−1139.
(33) Golden, D. C.; Dixon, J. B.; Chen, C. C. Ion Exchange, Thermal Transformations, and Oxidizing Properties of Birnessite. *Clays Clay Miner.* **1986**, *34*, 511−520.
(34) Johnson, E. A.; Post, J. E. Water in the Interlayer Region of Birnessite: Importance in Cation Exchange and Structural Stability. *Am. Mineral.* **2006**, *91*, 609−618.
(35) Sverdrup, H. U.; Johnson, M. W.; Fleming, R. H. *The Oceans: Their Physics, Chemistry, and General Biology*; Prentice-Hall: NY, 1942; Vol. 7.
(36) Feng, Q.; Liu, L.; Yanagisawa, K. Effects of Synthesis Parameters on the Formation of Birnessite-type Manganese Oxides. *J. Mater. Sci. Lett.* **2000**, *19*, 1567−1570.
(37) Feng, Q.; Kanoh, H.; Miyai, Y.; Ooi, K. Metal Ion Extraction/Insertion Reactions with Todorokite-type Manganese Oxide in the Aqueous Phase. *Chem. Mater.* **1995**, *7*, 1722−1727.
(38) Choi, H. S.; Kim, S. J.; Kim, J. J. Dehydration Behaviors of Interlayer Water in Synthetic Buserites. *Geosci. J.* **2004**, *8*, 273−279.
(39) Biesheuvel, M.; Zhao, R.; Porada, S.; van der Wal, A. Theory of Membrane Capacitive Deionization Including the Effect of the Electrode Pore Space. *J. Colloid Interface Sci.* **2011**, *360*, 239−248.
(40) Marcus, Y. Ionic Radii in Aqueous Solutions. *Chem. Rev.* **1988**, *88*, 1475−1498.
(41) Yin, J.; Takeuchi, E. S.; Takeuchi, K. J.; Marschilok, A. C. Synthetic Control of Manganese Birnessite: Impact of Crystallite Size on Li, Na, and Mg Based Electrochemistry. *Inorg. Chim. Acta* **2016**, *453*, 230−237.
(42) Luo, J.; Suib, S. L. Preparative Parameters, Magnesium Effects, and Anion Effects in the Crystallization of Birnessites. *J. Phys. Chem. B* **1997**, *101*, 10403−10413.
(43) Xing, F.; Li, T.; Li, J.; Zhu, H.; Wang, N.; Cao, X. Chemically Exfoliated MoS_2 for Capacitive Deionization of Saline Water. *Nano Energy* **2017**, *31*, 590−595.
(44) Gao, X.; Omosebi, A.; Landon, J.; Liu, K. Surface Charge Enhanced Carbon Electrodes for Stable and Efficient Capacitive Deionization Using Inverted Adsorption-Desorption Behavior. *Energy Environ. Sci.* **2015**, *8*, 897−909.
(45) Krishnamoorthy, K.; Veerapandian, M.; Yun, K.; Kim, S.-J. The Chemical and Structural Analysis of Graphene Oxide with Different Degrees of Oxidation. *Carbon* **2013**, *53*, 38−49.
(46) Moreno-Castilla, C.; Ferro-Garcia, M.; Joly, J.; Bautista-Toledo, I.; Carrasco-Marin, F.; Rivera-Utrilla, J. Activated Carbon Surface Modifications by Nitric Acid, Hydrogen Peroxide, and Ammonium Peroxydisulfate Treatments. *Langmuir* **1995**, *11*, 4386−4392.
(47) Clites, M.; Pomerantseva, E. Bilayered Vanadium Oxides by Chemical Pre-intercalation of Alkali and Alkali-earth Ions as Battery Electrodes. *Energy Storage Mater.* **2018**, *11*, 30−37.
(48) Pomerantseva, E.; Gogotsi, Y. Two-dimensional Heterostructures for Energy Storage. *Nat. Energy* **2017**, *2*, No. 17089.
(49) Wang, G.; Dong, Q.; Wu, T.; Zhan, F.; Zhou, M.; Qiu, J. Ultrasound-assisted Preparation of Electrospun Carbon Fiber/Graphene Electrodes for Capacitive Deionization: Importance and Unique Role of Electrical Conductivity. *Carbon* **2016**, *103*, 311−317.

DOI: 10.1021/acsami.8b09638
ACS Appl. Mater. Interfaces 2018, 10, 32313−32322